Wilkley Bezerra Correia[1], Rômulo Nunes de Carvalho Almeida[2], Wellington Assunção da Silva[3], Bismark Claure Torrico[3], Vandilberto Pereira Pinto[2], Laurinda L. N. dos Reis[3]

Universidade Federal do Ceará - Computer Engineering Course (1),
Universidade Federal do Ceará - Electrical Engineering Course (2),
Universidade Federal do Ceará - Department of Electrical Engineering (3)

The T-polynomial approach for LQG control applied to a Switched Reluctance Motor (SRM)

Abstract. This paper proposes a tuning procedure that combines the well known T-polynomial, from predictive control, with the LQG algorithm. The proposed scheme was successfully applied to a speed loop of a switched reluctance motor (SRM), which is known by its specific issues related to driving and control. Such characteristics make the SRM a strong set up to exploit the proposed solution. Results are compared with both the predictive controller approach GPCBC and the classical LQG/LTR, analysed regarding the transient and disturbance rejection. Power analysis of the control signal shows a power efficiency improvement favourable for the proposed approach.

*Streszczenie. Opisano sposób sterowania silnikiem reluktancyjnym wykorzystująca metodę T-wielomianu z algorytmem LQG – linear quadratic Gaussian. Metodę porównano z innymi metodami jak GPCBC I LQG/LTR pod kątem tłumienia zakłóceń i stanów chwilowych. **T-wielomianowa metoda sterowania przełączalnym silnikiem reluktancyjnym***

Keywords: T-polynomial, LQG control, Switched Reluctance Motor (SRM).
Słowa kluczowe: T-wielomian, silnik reluktancyjny, sterowanie LQG.

Introduction

It is well know that due to its constructive simplicity, inherent robustness, high torque density and potential for low-cost large scale production, switched reluctance motors (SRM) are now a modern alternative regarding electromechanical conversion on a variable speed solution [1,2]. For high performance applications, the SRM usually operates under magnetic saturation condition [3]. Such characteristics leads the motor into a strongly nonlinear behaviour [4], with several challenges to both constructive and control investigation, e. g. torque ripple minimization, wide range speed operation adjustment, fault tolerant drive control and acoustic noise reduction.

For low speed condition, current set-point tracking is mandatory for a proper speed and/or torque control [5]. However, at high speed operation, current control is constrained because driving circuit phases are switched on during a time window smaller than that of the rising time. As a consequence, current of the SRM may not reach the desired reference and current control is reduced for a single pulse command. Therefore, it is imperative one to consider robustness for the speed controller design in order to deal with both low and high speed operation, as well as it should guarantee disturbance rejection. Such requirements make speed control design a challenging task [6].

In order to accommodate such issues and provide feasible solutions to embedded real-time control, several approaches using intelligent controllers have been proposed. Many of these algorithms apply Optimized Search Algorithms, Fuzzy logic and Neural Networks [7, 8, 9]. However, predictive and robust controllers have more recently justified their application for this type of problem [5, 10], as them allow an analytical solution for disturbance rejection, transient response.

Within this context, this paper presents studies based on predictive and optimal control perspectives for speed control loop of a SRM. Under predictive control framework a control technique, based on the Generalized Predictive Control (GPC), named GPCBC [5], has been recently and successfully applied for the SRM's current loop. Such algorithm is extended herein for the speed control loop. The optimal control perspective considers the traditional Loop Transfer Recovery (LTR) technique, applicable for the Linear Quadratic Gaussian (LQG) control [11]. In this work

LQG/LTR is implemented for discrete-time, for comparison purposes with the proposed LQG algorithm based on the so called T-polynomial, commonly applied for GPC to improve robustness. Simulations were performed in order to show the effectiveness of the proposed control method regarding to both high noise frequency and step-like disturbances rejection. Additionally, power analysis of the control signal was considered for efficiency aspects investigation purposes.

Controllers that reached best simulation results were then implemented in a 6/4 SRM experimental setup (see Table 9 at the appendix for motor's details) in order to experimentally validate the results.

This paper is divided as follows. Next section presents description and identification of the speed model of the SRM. Middle section describes the LQG controller with T-polynomial proposed in this work. Last sections show simulations and experimental results followed by the conclusions of the paper.

Modelling and Identification of speed loop

Speed model of SRMs closely relates electromagnetic and mechanical variables. For the particular case of speed control, the block diagram shown in Fig. 1 is commonly reported [3].
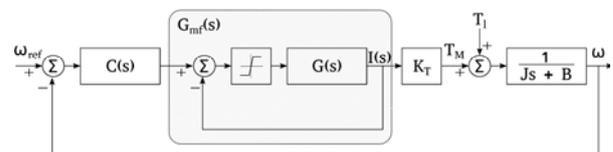

Fig. 1. Simplified block diagram of the Switched Reluctance Motor.

Transfer function *G(s)* in Fig. 1, at the inner loop, raises from the electric and magnetic characteristics of the motor. If current control loop is able to successfully track current reference, from low speed to single pulse operation at higher speeds, then the overall *Gmf(s)* may be modelled as a first order system such as:

(1)
$$G_{mf}(s) = \frac{K}{s+K}.$$

Mechanical part of the SRM relates moment of inertia J and viscous coefficient B, which is also a first order model given by:

$$(2) \qquad G_{mec}(s) = \frac{1}{Js + B}.$$

Therefore, the system to be controlled is a second order type, as follows:

$$(3) \qquad G_{SRM}(s) = \frac{K}{s + K} \frac{1}{Js + B}.$$

Current output $i(t)$ and mechanical conjugate T_m are related to each other through the gain relationship K_T shown in Fig. 1, given by [3]:

$$(4) \qquad T_M = \frac{1}{2} \frac{dL(\varphi)}{d\varphi} i^2,$$

where $\dfrac{dL(\varphi)}{d\varphi}$ is a constant, named inductance variation gradient, commonly referred to as κ [3].

Therefore, by applying equation (4) into equation (3), the model of the SRM may be written as:

$$(5) \qquad G_{SRM}(s) = \frac{K_v}{as^2 + bs + 1}.$$

This is a typical second order model whose parameters a, b and K_v may be obtained by a grey box identification method. In this work, it has been applied an identification based on non linear optimization with constraints, to obtain the discrete-time model, considering the sampling period $T_s = 0.1$ s and a zero-order holder, given by

$$(6) \qquad G_{SRM}(s) = \frac{0.3032z + 2.89 * 10^{-6}}{z^2 - 0.9048z}.$$

Equation (6) has one pole closer to the unit circle and one fast pole placed at zero. Such pole placement clearly distinguishes the slow dynamics, due to mechanic part of the model ($z=0.9048$), and the fast dynamics, due to electromagnetic part of the model ($z=0$). Thus, as the independent term of the numerator in equation (6) is nearly zero, it is suitable to consider the first order model:

$$(7) \qquad G_{SRM}(s) = \frac{0.3032}{z - 0.9048}.$$

LQG with T-polynomial

Consider a linear discrete-time system given by the CARIMA (Controller Auto-Regressive Integrative Moving Average) model:

$$(8) \quad A(z^{-1})y(k) = B(z^{-1})u(k-1) + C(z^{-1})\frac{w(k)}{\Delta},$$

where $\Delta = 1 - z^{-1}$, $y(k)$ and $u(k)$ stand for the system's output and input respectively. The additive disturbance $w(k)$ is a white gaussian noise and polynomials $A(z^{-1})$, $B(z^{-1})$ and $C(z^{-1})$ describe the model dynamics, given by:

$$A(z^{-1}) = 1 + a_1 z^{-1} + a_2 z^{-2} + \cdots + a_n z^{-n};$$
$$B(z^{-1}) = b_0 + b_1 z^{-1} + b_2 z^{-2} + \cdots + b_m z^{-m};$$
$$C(z^{-1}) = 1 + c_1 z^{-1} + c_2 z^{-2} + \cdots + c_{nc} z^{-nc},$$

where $n_c = n > m$. However, to identify the polynomial $C(z^{-1})$, that describes disturbance dynamics, is not always an easy task [12]. Therefore, $C(z^{-1})$ is often replaced by the so called T-polynomial, which is tuned to improve controller's robustness and may be given by

$$(9) \qquad T_{pol}(z^{-1}) = \left(1 - \alpha z^{-1}\right)^n$$

where α is the zero of the polynomial, acting as a tuning parameter. Details for a proper setting may be found in [12, 13].

On the other hand, robustness in the optimal control research is taken with a different perspective, where the LQG/LTR in the remarkable work reported by Doyle [11] plays a key role. Although it became a popular technique, recovery is guaranteed for minimal phase systems at continuous time, with additional conditions for discrete-time reported by [14].

So that, robustness under predictive and optimal control perspectives seems do not regard a closer relationship. However, Park et al. [15] have shown that a GPC with T-polynomial may be written as a Receding Horizon Controller (RHC) and a Kalman Filter.

In order to obtain a state space representation in terms of $u(k)$ instead of $\Delta u(k)$, in this work we take the T-polynomial in equation (9) as the multiplicative term of $w(k)$, replacing $C(z^{-1})/\Delta$ in equation (8), as integral action is taken by the state augmentation.

Then, the model takes the state space representation

$$(10) \quad \mathbf{x}(k+1) = \mathbf{A}\mathbf{x}(k) + \mathbf{B}u(k) + \mathbf{E}w(k);$$

$$(11) \quad y(k) = \mathbf{C}\mathbf{x}(k) + w(k),$$

where the system matrices are given by

$$\mathbf{A} = \begin{bmatrix} -a_1 & 1 & 0 & \cdots & 0 \\ -a_2 & 0 & 1 & \cdots & 0 \\ \vdots & \vdots & \vdots & \ddots & \vdots \\ -a_{n-1} & 0 & 0 & \cdots & 1 \\ -a_n & 0 & 0 & \cdots & 0 \end{bmatrix}, \quad \mathbf{B} = \begin{bmatrix} b_1 \\ b_2 \\ \vdots \\ b_m \end{bmatrix},$$

$$\mathbf{C} = \begin{bmatrix} 1 & 0 & \cdots & 0 \end{bmatrix}, \quad \mathbf{E} = \begin{bmatrix} t_1 - a_1 \\ t_2 - a_2 \\ \vdots \\ t_n - a_n \end{bmatrix}.$$

If an output disturbance $v(k)$ is also considered at the output of the state space model, then equations (10) and (11) may be written in the more general representation:

$$(12) \qquad \mathbf{x}(k+1) = \mathbf{A}\mathbf{x}(k) + \mathbf{B}u(k) + \mathbf{E}w(k);$$

$$(13) \qquad y(k) = \mathbf{C}\mathbf{x}(k) + \mathbf{F}w(k) + v(k);$$

where $w(k)$ and $v(k)$ are gaussian, uncorrelated processes with zero mean ($E\{w(k)\}=0$, $E\{v(k)\}=0$) and covariance matrices given by $E\{w(k)w^T(k)\} = R_w$, $E\{v(k)v^T(k)\} = R_v$ and $E\{w(k)v^T(k)\} = 0$. In a case where $\mathbf{F}=1$ and $v(k)=0$, then equation (13) becomes Eq. (11).

Note that the total output disturbance in equation (13) is $\xi_y(k) = Fw(k) + v(k)$, and state disturbance in equation (12) is $\xi_x(k) = \mathbf{E}w(k)$, which are clearly correlated signals. Hence, the Kalman gain expression has to be considered for such condition (see for instance [16]). So that one can find the Kalman gain expression:

$$(14) \qquad \mathbf{K}_{f_d} = \left(\mathbf{A}\mathbf{P}\mathbf{C}^T + \mathbf{E}R_w\mathbf{F}^T\right) \times$$
$$\left(\mathbf{C}\mathbf{P}\mathbf{C}^T + R_v + \mathbf{F}R_w\mathbf{F}^T\right)^{-1},$$

where P is the unique solution of the Riccati equation:

$$\mathbf{P} = \mathbf{A}\mathbf{P}\mathbf{A}^T + \mathbf{E}R_w\mathbf{E}^T - \left(\mathbf{A}\mathbf{P}\mathbf{C}^T + \mathbf{E}R_w\mathbf{F}^T\right) \times$$

$$\left(\mathbf{CPC}^{\mathrm{T}}+R_v+\mathbf{FR}_{\mathrm{w}}\mathbf{F}^{\mathrm{T}}\right)\left(\mathbf{APC}^{\mathrm{T}}+\mathbf{ER}_{\mathrm{w}}\mathbf{F}^{\mathrm{T}}\right)^{-1}.$$

Kalman gain given by equation (14) is applied to obtain the optimal state observer:

(15) $\hat{\mathbf{x}}(k+1)=\mathbf{A}\hat{\mathbf{x}}(k)+\mathbf{B}u(k)+\mathbf{K}_{\mathbf{f_d}}\left[y(k)-\hat{y}(k)\right],$

where $\hat{y}(k)=\mathbf{C}\hat{\mathbf{x}}(k)$. In order to complete the LQG control, state estimation $\hat{\mathbf{x}}(k)$ is fed back through the optimal gain $\mathbf{K_r}$ obtained from the Linear Quadratic Regulator (LQR) problem, given by:

(16) $\mathbf{K_r}=\left(\mathbf{B'}^{\mathrm{T}}\mathbf{SB'}+\mathbf{R}\right)^{-1}\mathbf{B'}^{\mathrm{T}}\mathbf{SA'},$

Where $\mathbf{S}$ is the unique solution of the Riccati equation:

$$\mathbf{S}=\mathbf{A'}^{\mathrm{T}}\mathbf{SA'}-\mathbf{A'}^{\mathrm{T}}\mathbf{SB'}[\mathbf{B'}^{\mathrm{T}}\mathbf{SB'}+\mathbf{R}]^{-1}\mathbf{B'SA'}+\mathbf{Q},$$

and $\mathbf{Q}$ and $\mathbf{R}$ are weighting matrices associated with the state and control. In order to include integral action (see [17] and [18] for details), it might be considered the augmented state $\mathbf{x_a}(k)=[\mathbf{x(k)}\ \mathbf{x_i(k)}]^T$, where $\mathbf{x(k)}$ is the state of the system and $\mathbf{x_i(k)}$ is the state related with integral action. In this case, matrices $\mathbf{A'}$ and $\mathbf{B'}$ are

$$\mathbf{A'}=\begin{bmatrix}\mathbf{A}&\mathbf{0}\\-\mathbf{C}&\mathbf{I}\end{bmatrix}\quad\text{and}\quad\mathbf{B'}=\begin{bmatrix}\mathbf{B}\\\mathbf{0}\end{bmatrix}.$$

The classical LQG/LTR technique considers that disturbance is added at the input of the system. So that, covariance matrix is given by $R_w=q^2\mathbf{BB}^{\mathrm{T}}$, which represents a fictitious noise intensity, with $q\in\mathbf{Re}$ and $q>0$ being a scalar. However, in this work it is considered that such noise intensity is weighted by $\mathbf{E}$ matrix in equation (12), leading to $R_w=\mathbf{EE}^{\mathrm{T}}$.

Robustness is improved for the LTR procedure as $q\rightarrow\infty$ [11]. For the controller proposed in this work, robustness is modified by the pole placement of the T-polynomial, which affects matrix $\mathbf{E}$, so that, tuning parameter α in equation (9) plays a fundamental role.

It is important to highlight that the choice of α is different for the GPC-T and for the LQG with T-polynomial (named here LQG-T to simplify writings). Under predictive control framework, T-polynomial is a low-pass filter and directly affects disturbance-to-output transfer function. On the other hand, for the LQG-T, $T(z^{-1})$ is a tuning parameter as a whole which modifies the Kalman gain $\mathbf{K_{fd}}$ and consequently, the poles of the observer. In other words, α is a tuning parameter that indirectly affects robustness, in contrary with GPC. Therefore, pole placement for T-polynomial is different for GPC and LQG-T control, as it becomes clear in the next section through simulations for the SRM. Additionally, an experimental result is presented in order to validate the proposed controller for an embedded application.

Simulation Results

In this section, simulations of GPCBC, LQG-T and LQG/LTR controllers were performed. The GPCBC controller's robustness is formulated with basis on the T-polynomial, which makes it suitable for comparative results with LQG-T. The GPCBC algorithm results in a RST structure whose polynomials are given by [5]:

(17) $\qquad T(z^{-1})=\dfrac{(1-\alpha_g)C(z^{-1})}{b_0};$

(18) $\qquad R(z^{-1})=1-\alpha_g c_2 z^{-1};$

(19)
$$S(z^{-1})=\frac{2-\alpha_g+c_1+\alpha_g c_2-\left[1+\alpha_g c_1+(2\alpha_g-1)c_2\right]z^{-1}}{b_0};$$

where b_0 is the numerator of the discrete-time transfer function of the plant and α_g is a tuning parameter which varies from 0 to 1. The T-polynomial, also referred to as T-filter, is described by $C(z^{-1})=1+c_1 z^{-1}+c_2 z^{-2}$, in order to avoid confusing notation with $T(z^{-1})$ defined above for the RST structure. So that, it is preferred to call $C(z^{-1})$ as a filter that improves robustness, which is given by

$$C(z^{-1})=\left(1-e^{-(\sigma+j\beta)}z^{-1}\right)\left(1-e^{-(\sigma-j\beta)}z^{-1}\right),$$

where σ and β and are tuning parameters which define complex conjugate roots at continuous time: $s_r=\sigma\pm j\beta$. The main idea consists in choose an absolute value for s_r and vary the angle of s_r, which makes σ and β to vary for each desired angle.

In the previous work Torrico et. al. [5] have shown that the choice $\beta=\sigma$ ($45°$ for s_r) reaches an acceptable trade-off between disturbance rejection and noise attenuation, as well as it also speeds up step disturbance signals for the current control loop. In this work the same GPCBC is applied to control the speed loop, which is about 1000 times slower than the current loop. As a consequence, tuning parameters had to be modified to $\sigma=0.1$ and $\alpha_g=0.905$, in order to guarantee both good performance regarding to the disturbance rejection and noise attenuation. Such choice place the poles of $C(z^{-1})$ at $z=0.9048$ and $z=0.9048e^{\pm j0.1}$ for $0°$ and $45°$, respectively, in s-plane. Therefore,

$$C_0(z^{-1})=1-1.8096z^{-1}+0.81871z^{-2}$$

and

$$C_{45}(z^{-1})=1-1.8006z^{-1}+0.81871z^{-2}.$$

It is worthy to note that the poles of $C_{45}(z^{-1})$ are just about $5.7°$ in the z-plane.

The pole placement of the poles of the filter $C(z^{-1})$ has direct influence on the disturbance rejection. On the other hand, pole placement in the LQG-T algorithm have an indirect influence, as T-polynomial plays the role of a tuning parameter which modifies the Kalman gain in the Kalman filter. Therefore, one might not expect the poles of $C(z^{-1})$ and $T_{LQG-T}(z^{-1})$ to be equal. In this work, although the absolute value is the same for the poles of both algorithms, the angles are different. So that, LQG-T has been tuned to place the poles of $T_{LQG-T}(z^{-1})$ at $z=0.9048$ and $z=0.9048e^{\pm j0.6981}$, whose angle is about $40°$ in the z plane, to obtain

$$T_{LQG-T_0}(z^{-1})=1-1.81z^{-1}+0.82z^{-2}$$

and

$$T_{LQG-T_{40}}(z^{-1})=1-1.39z^{-1}+0.82z^{-2}.$$

The robustness analysis criteria consider the upper bound $\overline{\delta_p}$ multiplicative error of 10% gain uncertainty and two samples of variation in time delay, as performed in [15]. Fig. 2 shows that GPCBC$_{45°}$ and LQG-T$_{40°}$ present almost the same robustness behaviour up to 11 rad/s. For frequencies higher than that $I_r(j\omega)$ graphs for both controllers separate each other. Particularly, $\overline{\delta_p}$ is closer to be violated for frequencies between 8 rad/s and 11 rad/s, where GPCBC$_{45°}$ and LQG-T$_{40°}$ are equivalent.

All the simulations of this section consider a 10 s of total time with a step input disturbance $d_{in}=300$ applied at $t=3$ s and white noise with power 1 applied in $t=5$ s. Additionally, a 40 Hz sinusoidal disturbance signal was added for the total simulation time, in order to reproduce a real

disturbance signal noticed in the real case, maybe due to electromechanical intrinsic characteristic of the SRM.
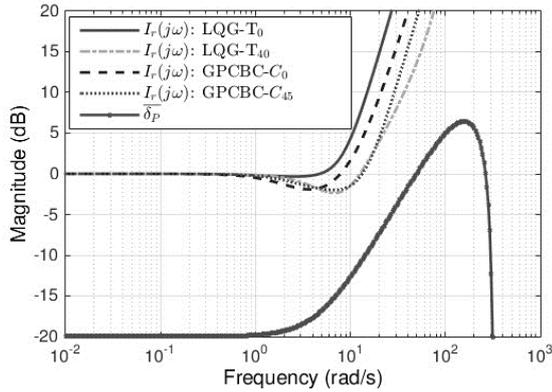

Fig. 2. Robustness analysis for 10% gain uncertainty and two samples of time delay uncertainty.

Comparison between GPCBC(0°) and GPCBC(45°)

A preliminary comparison study is presented for GPCBC by considering two different cases: $C_0(z^{-1})$ and $C_{45}(z^{-1})$. Note that Fig. 3 shows clearly that the GPCBC$_{45°}$ significantly speeds up disturbance rejection compared to GPCBC$_{0°}$, as can be seen by the detail at *3 s*. A quantitative analysis of this behaviour is given in Table 1, by the performance indices [19]: Integrated Absolute Error (IAE) and Total Variation (TV) for set-point reference tracking (SR) and load disturbance rejection (LDR). By looking at the IAE-LDR index one can notice the smaller value for the *45°* case, which indicates its improvement regarding step-like disturbance rejection. On the other hand, the smaller TV indices for the GPCBC$_{0°}$ case indicate its better performance regarding the control signal for both the transient operation (see TV-SR indices and current graphs in Fig. 1 for *0 < t < 2 s*) and disturbance rejection (see TV-LDR indices and current graphs in Fig. 1 for *3 < t < 5 s*).
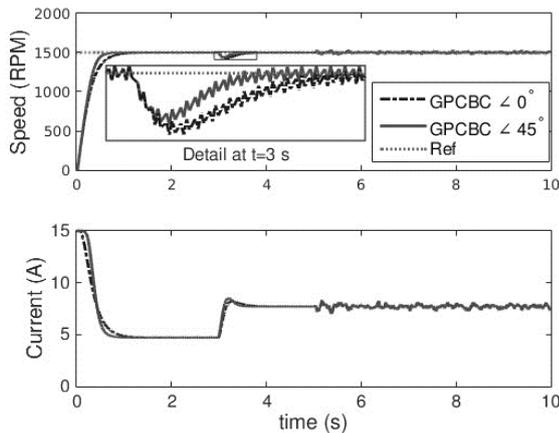

Fig. 3. Simulation step response (GPCBC angle 0° and GPCBC angle 45°).

Table 1. Performance indices: experimental results

Controller	IAE		TV	
	SR	LDR	SR	LDR
GPCBC∠0°	382.90	34.61	1806.98	1432.62
GPCBC∠45°	328.04	23.34	2161.94	1851.86

Performance indices aforementioned are a consistent tool usually applied to concisely report the controller's performance regarding set-point tracking and disturbance rejection. However, output variations, such as low and high

frequency noise, may reflect in control actions. In this case, variance (VAR) has been usually applied as an index to quantify the long-term behaviour with a single value, and could be used as a power signal indicator.

Regarding to power analysis, the power spectral density (PSD) is a frequency portrait of a signal that contains information related to its power. By integrating the PSD graph over a frequency range one gets the total power of the signal under analysis (see [20] for more details about PSD).

In the case of control systems, PSD applied to the control signal offer a graphic view of its power. In addition, total power computed is a concise measure of efficiency that complements the VAR index.

For the simulations and experimental results carried out, a spectral analysis of the control signal was performed. For such purpose, it has been considered $u(t)$ for $t \geq 5\ s$ (when the white noise has been added). The DC level has been taken out by subtracting the average level of the control signal in the mentioned time interval, producing the signal.

$$(20) \qquad u_0(k) = u(k) - \bar{u},$$

where $\bar{u} = \dfrac{1}{M}\sum_{j=0}^{M} u(j)$ and M is the total number of samples of the signal $u(k)$ over the time interval ($t \geq 5\ s$ in this particular case).

However, $u_0(k)$ is a discrete-time signal and PSD is estimated for a continuous range of frequencies. So that is necessary to take into account the relationship $z = e^{j\omega T_s}$, $0 < \omega \leq \dfrac{\pi}{T_s}$, where T_s is the sampling time, i.e. ,

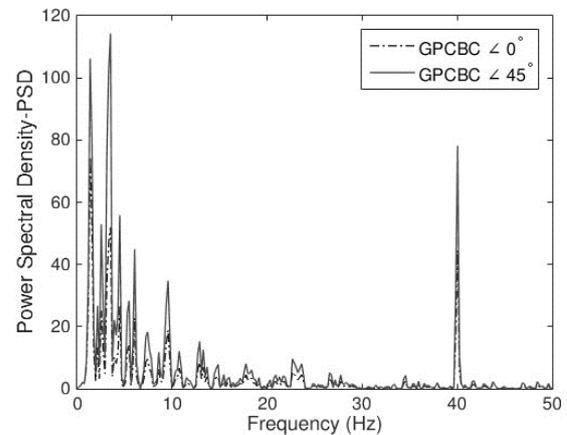PSD can be estimated for $u_0(k)$ over $0 < \omega \leq \dfrac{\pi}{T_s}$.

Fig. 4. Frequencies related to $u_0(t)$ ($t \geq 5$) for the current control signals in Fig. 3.

PSD graphs for GPCBC controllers are shown in Fig. 4. Although GPCBC$_{45°}$ shows a better performance regarding to load disturbance rejection, GPCBC$_{0°}$ clearly presents power peaks lower than the 45° case in almost all frequencies.

The total power column in Table 2 are in accordance with the initial analysis of the PSD peaks mentioned earlier for the 0° case, which are in accordance with the computed variance (see column VAR), and indicates a better performance for steady-state. Note that results in Table 2 are regarding to the steady state analysis ($5 < t < 10\ s$), and keep no relationship with results in Table 1. Same applies to the related tables in next sections.

Besides, the main purpose of the GPCBC$_{45°}$ is to accelerate disturbance rejection, which is commonly a desirable behaviour, especially for electric motor operation purposes, like this case study.

Table 2. Power Analysis: experimental results

Controller	Total Power	VAR
GPCBC∠0°	54.66	196.18
GPCBC∠45°	100.65	373.69

Comparison between LQG/LTR and LQG-T(40°)

In the following, the proposed LQG-T controller is compared with the traditional LQG/LTR implemented in discrete-time. The LQG/LTR has been tuned with $q = 100$ in order to achieve disturbance rejection as fast as the one obtained for the GPCBC-$45°$. Both controllers were set with $\mathbf{R} = 20$ and $\mathbf{Q} = \mathbf{C_a}^T\mathbf{C_a}$, where $\mathbf{C_a} = [\mathbf{C}\ \mathbf{I}]$, in order to guarantee the same reference tracking behaviour.

In Fig. 5 it is noticed that disturbance rejection is very similar for both controllers, as detailed at $t = 3\ s$. On the other hand, control signal graphs clearly show that the behaviour of the LQG-T controller is smoother than that of the LQG/LTR (see detail at $t = 5.5\ s$).
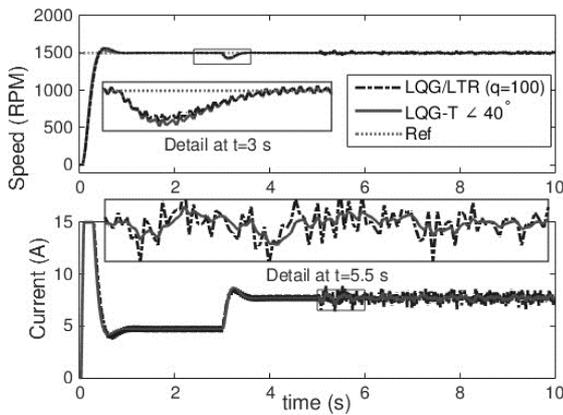

Fig. 5. Simulation step response (LQG/LTR - q=100 and LQG-T angle 40°).
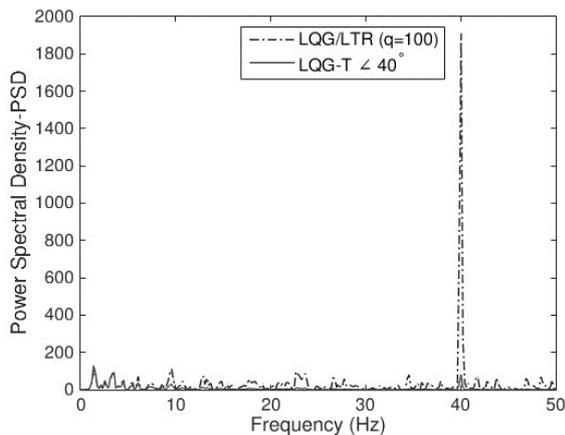

Fig. 6. Frequencies related to $u_0(t)$ ($t \geq 5$) for the current control signals in Fig. 5.

In Fig. 6 it can be seen that frequency peaks of the LQG-T controller are almost equal the ones of the LQG/LTR for lower frequencies, but are strongly reduced for higher frequencies. Special attention must be paid for the strongly increment of power at *40 Hz* for the LQG/LTR, while LQG-T keeps it at the same level of the low frequency ones.

Step response in Fig. 5 is quantified by the indices shown in Table 3, where IAE indices regarding to the output (speed) indicate a similar behaviour of both controllers for the transient (IAE-SR) and disturbance rejection (IAE-LDR). However, TV-LDR and TV-SR indices of the LQG-T are respectively about a quarter and a half of that of the LQG/LTR, which clearly indicates that the LQG-T control signal exhibits smaller variation than the LQG/LTR one. This is a desired behaviour as smoothness in control signal has direct influence on actuators operation.

Table 4 quantify the spectral behaviour by showing that the total power of of the LQG-T controller is about a fifth of that of the LQG/LTR one. Total variance is also favourable for the LQG-T controller which is in accordance with the total power values.

Table 3. Performance indices: experimental results

Controller	IAE		TV	
	SR	LDR	SR	LDR
LQG/LTR (q=100)	344.81	26.36	8817.47	8256.77
LQG-T∠40°	328.48	28.33	3794.11	1917.57

Table 4. Power Analysis: experimental results

Controller	Total Power	VAR
LQG/LTR (q=100)	522.88	1743.03
LQG-T∠40°	95.27	324.14

Comparison between LQG-T(40°) and GPCBC(45°)

In order to complete the analysis, the proposed LQG-T, tuned as in the previous section, is compared with the GPCBC$_{45°}$, tuned as in the previous comparison with GPCBC$_{0°}$. The aim of this comparative study is to determine which controller reaches the better trade-off between disturbance rejection indices and steady state behaviour.

Step response in Fig. 7 shows that the step-like disturbance rejection is slightly improved for GPCBC$_{45°}$, with similar set-point reference for both controllers.
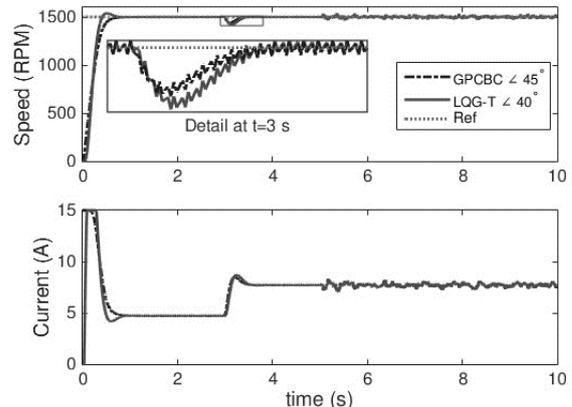

Fig. 7. Simulation step response (GPCBC angle 45° and LQG-T angle 40°).

On the other hand, Fig. 8 shows that the LQG-T controller exhibits lower peaks of the PSD at the majority of the lower frequencies and roughly the same peak of the GPCBC controller at the undesirable *40 Hz* disturbance signal.

Step response behaviour is quantified in Table 5, which shows the similar behaviour of the compared controllers regarding to the set-point reference track (see IAE-SR index column), although TV-SR column indicates an advantage of the GPCBC over LQG-T as it exhibits a smoother control signal (see current graphs in Fig. 7 for *0 < t < 2 s*). In addition, TV-LDR index shows just a slightly better performance of GPCBC controller, nevertheless, a very small variation of the weight **R** for the LQG-T could lead to a different result, so that, it can be considered that both controllers exhibit similar behaviour regarding to disturbance rejection (see current graphs in Fig. 7 for *3 < t < 5 s*).
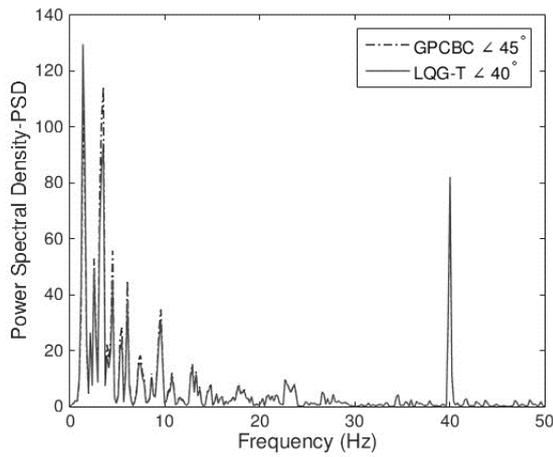
Fig. 8. Frequencies related to $u_0(t)$ ($t \geq 5$) for the current control signal in Fig. 7.

On the other hand, the power analysis in Table 6 shows that the LQG-T controller presents a more efficient result regarding the total power, despite of the close values.

Table 5. Performance indices: experimental results

Controller	IAE		TV	
	SR	LDR	SR	LDR
GPCBC∠45°	328.04	23.34	2161.94	1851.86
LQG-T∠40°	328.48	28.33	3794.11	1917.57

Table 6. Power Analysis: experimental results

Controller	Total Power	VAR
GPCBC∠45°	100.65	373.69
LQG-T∠40°	95.27	342.14

Experimental Results

This section provides an experimental application of the proposed controller, aiming both to show the effectiveness of the proposed control method and validate the GPCBC/LQG-T simulation comparison of the previous section. Thus, controllers were adjusted exactly as in the simulation.

The bench is assembled by a 6/4 SRM, switched by a three-phase power converter which is fed by a *120 V* voltage controlled source, as shown in Fig. 9. Driving circuit is controlled through a TI TMS320F28335 DSP, which contains the controller's codes considered in this work. Both the motor and the converter were designed at the Department of Electrical Engineering of the Universidade Federal do Ceará. The SRM is coupled to a generator cascaded with a rheostat, which plays the resistive load role. By varying the resistance one also varies the generator torque which reflects as a load torque disturbance for the reluctance motor. Therefore, it is considered a *20 W* resistive load in order to get a suitable torque for the motor's speed. However, the rheostat is manually added to the generator, which makes difficult to add disturbances at exactly *t = 3 s*.

Step response shown in Fig. 10 exhibits the output behaviour very similar of that obtained in the simulation for both set-point reference tracking and load disturbance rejection. Besides output and control signal graphs are apparently similar, in this case the IAE and TV indices become a more precise way to investigate the controllers' performance. Therefore, set-point reference, given by the IAE-SR and TV-SR indices shown in Table 7, exhibits an advantage for the LQG-T compared to the GPCBC. The load disturbance rejection indices are about a half of these observed from the simulation results in Table 5 and might be considered as equivalent to each other for this experimental test.
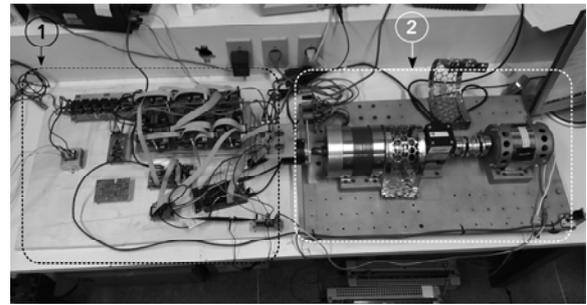

Fig. 9. Experimental bench set up. 1 - power converter (switching circuit). 2 - 6/4 Switched Reluctance Motor.

As performed for simulations, spectral analysis has also been taken for the experimental test considering $u_0(t)$ for *t≥5s*. Results can be seen in Fig. 11 where PSD peaks are smaller at lower frequencies for the LQG-T, although the *40 Hz* disturbance signal has almost the same peak value for both controllers. Nevertheless, the total power for the LQG-T controller is about a half of the GPCBC one, as presented in Table 8. The analysis may be complemented by the VAR column whose values for the comparative controllers follow the total power tendency. This restates the efficiency improvement of the proposed controller.
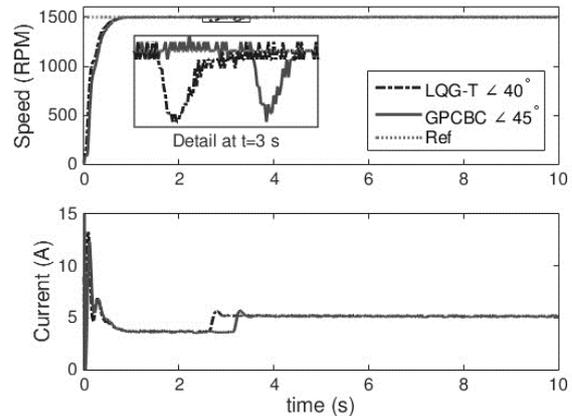

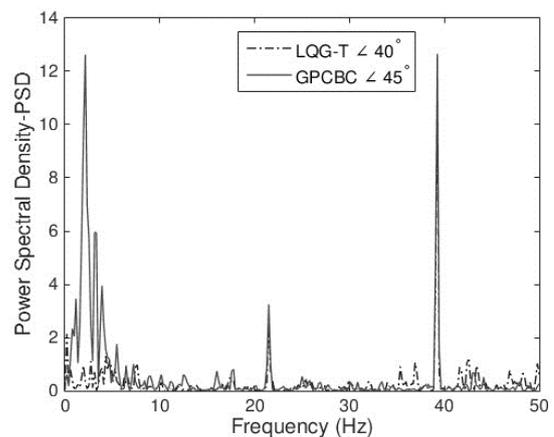Fig. 10. Step response: experimental results.

Fig. 11. Frequencies related to $u_0(t)$ ($t \geq 5$) for the current control signal in Fig. 10: experimental results.

Table 7. Performance indices: experimental results

Controller	IAE		TV	
	SR	LDR	SR	LDR
GPCBC∠45°	321.51	10.60	4397.00	923.00
LQG-T∠40°	258.17	13.50	4292.00	1008.00

Table 8. Power Analysis: experimental results

Controller	Total Power	VAR
GPCBC∠45°	8.84	23.91
LQG-T∠40°	4.60	16.06

Conclusion

This paper proposed a control tuning method applicable for LQG applied for a switched reluctance motor. The technique incorporates the so called T-polynomial, popular in the predictive control community, into the optimization problem of the Kalman filter, which results in the controller named herein as LQG-T. Simulations indicate that the proposed control method and the LQG/LTR controller exhibit similar results regarding to the speed control. Nevertheless, LQG-T improves the operation of the current actuators as its control signal is less oscillatory than that of the LQG/LTR. In addition, comparison results between LQG-T and GPCBC suggest that both controllers are equivalent with respect to the transient response (set-point reference tracking) and disturbance rejection. However, steady state analysis, which is investigated through power analysis of the control signal, indicates a slightly improvement favourable for the LQG-T compared with GPCBC. Experimental results for a 6/4 SRM workbench shows that indeed the transient response and disturbance rejection are similar for both controllers, while the power analysis at the steady state shows a better performance for the LQG-T over GPCBC, as it highlights the reduction of the total power computed. In the light of the promising results, a long term experiment is advised in order to validate the improvement on power efficiency of the control solution.

APPENDIX

Table 9. Main characteristics of the 6/4 SRM

Characteristic	Values
Number of phases	3
Nominal current (A)	10
Nominal Voltage (V)	120
Nominal speed (rpm)	1500
Stator resistance (Ω)	0.48
Maximum inductance (mH)	8
Minimum inductance (mH)	12
Poles per phase at the stator	2

Authors: *Wilkley Bezerra Correia, Rômulo Nunes de Carvalho Almeida, Vandilberto Pereira Pinto, Computer and Electrical Engineering courses at Sobral, Universidade Federal do Ceará - Campus Mucambinho, Rua Estanislau Frota, S/N, 62000 Sobral-CE, Brazil, email: wilkley,rnunes@dee.ufc.br,vandilberto@ufc.br, Wellington Assunção Silva, Bismark Claure Torrico, Dr., Laurinda L. N. dos Reis, Dr., Department of Electrical Engineering, Universidade Federal do Ceará – Campus do Pici, P.O.Box 6001 - Fortaleza-CE,Brazil, email: wellington,bismark,laurinda@dee.ufc.br*

REFERENCES
[1] Kiyota K., and Chiba A. Design of switched reluctance motor competitive to 60-kw ipmsm in third-generation hybrid electric vehicle. IEEE TRANSACTIONS ON INDUSTRY APPLICATIONS, 48:2303–2309, 2012.
[2] X. D. Xue, K. W. E. Cheng, J. K. Lin, Z. Zhang, K. F. Luk, T. W. Ng, and N. C. Cheung. Optimal control method of motoring operation for srm drives in electric vehicles. IEEE TRANSACTIONS ON VEHICULAR TECHNOLOGY, 59:1191–1204, 2010.
[3] T. J. E Miller. Electronic Control of Switched Reluctance Machines. Newnes, Oxford, UK, 2001.
[4] Wieslaw JAZDZYNSKI, Michal MAJCHROWICZ. Analytical Model of a Switched Reluctance Motor for its Optimization – Selected Problems. PRZEGLĄD ELEKTROTECHNICZNY, R. 89 NR 11/2013: 153-158, 2013.
[5] Torrico B. C., Almeida R. N. C, dos Reis L. L. N., Silva W. A., and Pontes R. S. T. Robust control based on generalized predictive control applied to switched reluctance motor current loop. Journal of Dynamic Systems, Measurement and Control, 136, 2012.
[6] Piotr. BOGUSZ. Analiza wpływu wybranych parametrów sterowania na właściwości napędu SRM pojazdu elektrycznego. PRZEGLĄD ELEKTROTECHNICZNY. R. 90 NR 2/2014: 161-164, 2014.
[7] Mehmet GEDIKPINAR. The speed control of DC motors with Support Vector Machine. PRZEGLĄD ELEKTROTECHNICZNY, R. 87 NR 5/2011: 269-271, 2011.
[8] X. D. Xue, K. W. E. Cheng, and S. L. Ho. Optimization and evaluation of torque-sharing functions for torque ripple minimization in switched reluctance motor drives. IEEE TRANSACTIONS ON POWER ELECTRONICS, 24:2076–2090, 2009.
[9] Christopher A. Hudson, N. S. Lobo, and R. Krishnan. Sensorless control of single switch-based switched reluctance motor drive using neural network. IEEE TRANSACTIONS ON INDUSTRIAL ELECTRONICS, 55:321–329, 2008.
[10] Prashanth Krishnamurthy, Wenzhe Lu, Farshad Khorrami, and Ali Keyhani. Robust force control of an srm-based electromechanical brake and experimental results. IEEE TRANSACTIONS ON CONTROL SYSTEMS TECHNOLOGY, 17:1306–1317, 2009.
[11] J. C. Doyle and G. Stein. Robustness with observers. IEEE Transactions on Automatic Control, 24(24):607–611, 1979.
[12] Eduardo Fernández Camacho and Carlos Bordons. Model Predictive Control. Springer-Verlag, London, UK, 2nd edition, 2004.
[13] J. A. Rossiter. Model-based predictive control: a practical approach. CRC Press, Boca Raton - Florida, USA, 2002.
[14] J. M. Maciejowski. Asymptotic recovery for discrete-time systems. IEEE Transactions on Automatic Control, 30(6):602–605,1985.
[15] Jung Jun Park, Soohee Han, and Wook Hyun Kwon. Finite memory generalized predictive controls for discrete-time state space models. In International Conference on Control, Automation and Systems - Seoul, Korea, 2008.
[16] Thomas Kailath, Ali H Sayed, and Babak Hassibi. Linear estimation, volume 1. Prentice Hall Upper Saddle River, NJ, 2000.
[17] Sigurd Skogestad and Ian Postlethwaite. MULTIVARIABLE FEEDBACK CONTROL: Analysis and design. John Wiley & Sons, New York, USA, 2 edition, 2005.
[18] Gene F. Franklin, J. David Powell, and Michael L. Workman. Digital Control of Dynamic Systems. Addison-Wesley, Menlo Park, CA, USA, 1997.
[19] Sigurd Skogestad. Simple analytic rules for model reduction and pid controller tuning. Journal of Process Control, (13):291–309, 2003.
[20] B. P. Lathi. MODERN DIGITAL AND ANALOG COMMUNICATION SYSTEMS. Oxford University Press. 1995. NY USA.